Inflammation and fibrosis in the coal dust-exposed lung described by confocal Raman spectroscopy

Wenyang Wang[1,2,3,4], Min Mu[1,2,3,4], Yuanjie Zou[1,2,4], Bing Li[1,2,4], Hangbing Cao[1,2,4], Dong Hu[1,2,3,4] and Xinrong Tao[1,2,3,4]

[1] Key Laboratory of Industrial Dust Control and Occupational Health of the Ministry of Education, Anhui University of Science and Technology, Huainan, Anhui, China
[2] Anhui Province Engineering Laboratory of Occupational Health and Safety, Huainan, Anhui, China
[3] Anhui University of Science and Technology, Key Laboratory of Industrial Dust Deep Reduction and Occupational Health and Safety of Anhui Higher Education Institutes, Huainan, Anhui, China
[4] Anhui University of Science and Technology, School of Medicine, Department of Medical Frontier Experimental Center, Huainan, Anhui, China

ABSTRACT

Background: Coal workers' pneumoconiosis (CWP) is an occupational disease that severely damages the life and health of miners. However, little is known about the molecular and cellular mechanisms changes associated with lung inflammation and fibrosis induced by coal dust. As a non-destructive technique for measuring biological tissue, confocal Raman spectroscopy provides accurate molecular fingerprints of label-free tissues and cells. Here, the progression of lung inflammation and fibrosis in a murine model of CWP was evaluated using confocal Raman spectroscopy.

Methods: A mouse model of CWP was constructed and biochemical analysis in lungs exposed to coal dust after 1 month (CWP-1M) and 3 months (CWP-3M) *vs* control tissues (NS) were used by confocal Raman spectroscopy. H&E, immunohistochemical and collagen staining were used to evaluate the histopathology alterations in the lung tissues.

Results: The CWP murine model was successfully constructed, and the mouse lung tissues showed progression of inflammation and fibrosis, accompanied by changes in NF-κB, p53, Bax, and Ki67. Meanwhile, significant differences in Raman bands were observed among the different groups, particularly changes at 1,248, 1,448, 1,572, and 746 cm^{-1}. These changes were consistent with collagen, Ki67, and Bax levels in the CWP and NS groups.

Conclusion: Confocal Raman spectroscopy represented a novel approach to the identification of the biochemical changes in CWP lungs and provides potential biomarkers of inflammation and fibrosis.

Subjects Biochemistry, Cell Biology, Toxicology, Public Health, Histology
Keywords Confocal Raman spectroscopy, Biochemical compositions, Collagen, Fibrosis, Lung inflammation, Coal workers' pneumoconiosis

INTRODUCTION

Coal workers' pneumoconiosis (CWP) develops from inhaling coal dust or mineral dust particles. As of 2018, there were 97,500 reported occupational diseases in China, and 90% of them were pneumoconiosis (*Yuan et al., 2022*). CWP patients have extensive fibrosis of the lung tissue, twisty, narrow, or distorted bronchi, and complications such as chronic obstructive pulmonary disease (COPD), which damages pulmonary function. In addition, coal dust particles in lung tissue can produce a variety of toxic effects, including oxidative stress, oxidative DNA damage, an acute stress reaction, and damage to large molecules such as lipoproteins (*León-Mejía et al., 2018*). The pathogenesis of CWP fibrosis has been reported to be the result of a continuous interaction between the coal dust particles and the chronic inflammatory response of the lung (*Perret et al., 2017*).

As a non-destructive technique for measuring biological tissue, confocal Raman spectroscopy provides accurate molecular fingerprints of label-free tissues and cells (*Li et al., 2020*). The spatial distribution of particular components is obtained by Raman spectroscopy, and 3D structural information from tissues has been constructed to identify each component of samples (*Kang, Nguyen & Lue, 2021*). Confocal Raman spectroscopy has been successfully used in tumor cell identification (*Wen et al., 2021*), stem cell research (*Hsu et al., 2020*), and the analysis of drug-resistant bacteria (*Lu et al., 2022*), and toxicology analysis (*Zitouni et al., 2020*). Several murine models of the effects of particulate matter on lung inflammation and damage have been constructed, with the types of particulate matter mainly including coarse and fine particulate matter, coal fly ash, and coal mine dust (*Albrecht et al., 2002*; *Finnerty et al., 2007*; *Happo et al., 2008*; *Hargrove et al., 2018*; *Lee et al., 2021b*). Our recent study reported confocal Raman spectroscopy to evaluate lung inflammation and injury in silicosis (*Wang et al., 2022*). We wonder if Raman spectroscopy could be extended to characterize other lung inflammation and fibrosis types, such as coal dust-induced inflammation and fibrosis.

In this study, an observation of pathological changes in lung tissue was carried out using a mouse model of CWP. Additionally, the changes in the nucleic acid, protein, and collagen of the mouse pneumoconiosis lungs were detected by Raman spectroscopy. We additionally analyzed the expression levels of NF-κB, p53, Bax, and Ki67 in lung tissues by immunohistochemical staining, finding that their levels were consistent with the Raman bands observed within the different groups. Thus, our work provides a novel approach for identifying the biochemical changes in lung tissues after coal dust exposure and represents a significant resource for understanding the mechanism of CWP.

MATERIALS AND METHODS

Animals and coal dust

All animal studies were carried out in accordance with the National Institutes of Health's Guide for the Care and Use of Laboratory Animals (NIH Publication No. 8023, revised 1978) and were approved by the Anhui University of Science and Technology's Institutional Animal Care and Use Committee (No. 2020006). Changzhou Cavion Experimental Animal Co., Ltd. (license number SCXY (Su) 2011-0003) provided six to

eight-week-old C57BL/6 male mice. The mice were housed in filtered-air ventilated cages with *ad libitum* access to food and drink in an environment with a 12-h light/dark cycle, temperature of 24 ± 1 °C, and humidity of 50 ± 5%.

Coal dust particles were collected in a coal mine in Anhui Province, China. The distribution of the particle size and the microelement content were analyzed in our previous study (*Mu et al., 2022*).

CWP mouse model

A CWP mouse model was established *via* the nasal inhalation of coal dust particles. The murine model was reported previously (*Mu et al., 2022*). Briefly, 20 mice were randomly divided into two groups: a control group (NS) and a coal dust exposure group. The mice were anesthetized by isoflurane inhalation and intranasally administered into the lung twice per week for 4 weeks (50 mg/ml/80 µl per week), and the NS group were administered saline (vehicle control). After 1 month, half of each group of mice was sacrificed. The experimental design is shown in Fig. 1.

Pulmonary function test

As described previously (*Sun et al., 2021*), mice were placed in a whole-body plethysmograph (WBP-4MR, Shanghai, China). After 30 min of acclimation in the cavity, inspiration time (Ti), tidal volume (Tv), expiration time (Te), and breath frequency were recorded by software (ResMass 1.4.2, Shanghai, China).

Lung tissue preparation

After determination of pulmonary function, mice were sacrificed by cervical dislocation and the lung tissues were obtained. The samples were placed on a tissue base mold and covered with cryo-embedding media for frozen sections. After that, the frozen tissue was sliced into 5 µm (Leica CM 1950; Leica Nussloch, Germany). The frozen sections were used for Raman spectroscopy analysis and pathological staining.

Raman instrumentation

To collect Raman data, we used an Alpha300R confocal Raman microscope with a 532-nm excitation laser diode (WITec, Ulm, Germany). A 100× objective (numerical aperture, 0.9; ZEISS, Oberkochen, Germany) for incident laser beam focusing was used to conduct Raman scattering measurements at a 2-cm^{-1} spectral resolution and 1,200-g/mm grating. With LabSpec six, all SCRS were preprocessed with comic ray correction and polyline baseline fitting (Horiba Scientific, Kyoto, Japan). The entire spectrum region was vector normalized for spectral normalization. Vector normalization was chosen to address general instrumentation variability and sample and experimental factors (*e.g.*, sample thickness) without significantly affecting the biological content. Normalizing a specific biocomponent was used to eliminate any presumptions of specific biomolecular alterations.
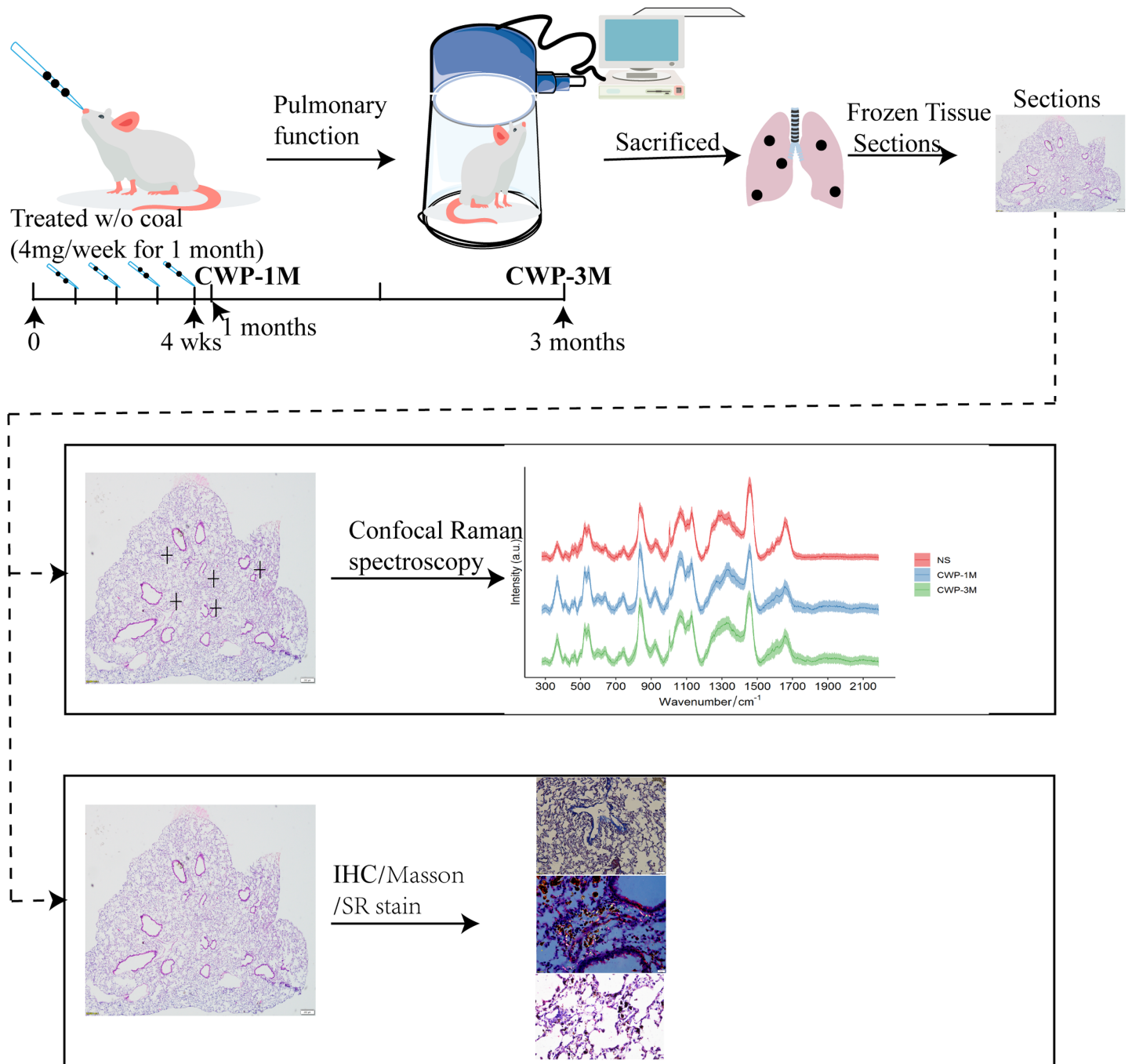
Figure 1 Experimental design. Mice were slightly anesthetized with isoflurane inhalation and coal dust particles were intranasally administered into their lungs at 4 mg/week for 4 weeks. Subsequently, the respiratory function of the mice was tested after 1 and 3 months before they were sacrificed. Lung tissue sections were obtained to evaluate changes in biochemical compositions using confocal Raman spectroscopy, in conjunction with immunohistochemistry and other staining methods.

Full-size ☑ DOI: 10.7717/peerj.13632/fig-1

Section staining

For hematoxylin and eosin (H&E) staining of frozen tissue sections, we used the standard H & E process. Briefly, we stained the tissue with Mayer's hematoxylin (C0105S; Beyotime,

Shanghai, China), rinsed them in distilled water for 5 min, and stained them with eosin (C0105S; Beyotime, Shanghai, China) for 7 min. Finally, the sections' dehydration, clearing, and sealing were conducted as standard.

For Masson's staining of frozen tissue sections, we used Masson's Trichrome Stain Kit (G1340; Solarbio, Beijing, China). Briefly, fixed frozen sections were rinsed three times in distilled water, submerged in Weigert's iron hematoxylin for 7 min, and washed twice with distilled water. Next, acid ethanol differentiation was conducted for 10 s, and the sections were then rinsed in distilled water. Ponceau S was used for 15 min, and the sections were twice washed with double distilled water. After that, the slices were stained for 10 min with phosphomolybdic acid solution. the solution was discarded, and the sections were stained with aniline blue solution for 5 min. Next, the sections were rinsed once for 2–3 s with double distilled water. Finally, dehydration, clearing, and sealing the sections were conducted as usual.

For Sirius Red staining of frozen tissue sections, we used a Sirius Red staining kit (SBJ-0294; SenBeiJia Biological Technology, Co., Ltd., Nanjing, China). Briefly, fixed frozen sections were rinsed three times in distilled water and then stained with picrosirius red solution for 60 min. Then, the slide was rinsed with acetic acid solution and stained with Mayer's hematoxylin for 10 min. Finally, dehydration, clearing, and sealing of the sections were performed as usual.

For immunohistochemical staining, fixed frozen sections were rinsed in distilled water three times, and the Quick Antigen Retrieval Solution (P0090; Beyotime, Shanghai, China) was used for antigen retrieval. Next, 3% bovine serum albumin was used to block nonspecific binding, and the sections were incubated at 4 °C overnight with anti-Ki67 antibody (ab15580; Abcam, Cambridge, UK; 1:500 dilution), anti-NF-κB (8242S; Cell Signaling Technology, Danvers, MA, USA; 1:1,000 dilution), anti-p53 (10442-1-AP; Proteintech, Rosemont, IL, USA; 1:200 dilution), and anti-Bax (26593-1-AP; Proteintech, Rosemont, IL, USA; 1:500 dilution). After three washes in phosphate-buffered saline, the slides were incubated with secondary antibodies (ImmPRESS®-AP Horse Anti-Mouse/ Rabbit IgG Polymer Detection Kit, Alkaline Phosphatase, MP-5402, MP-5401, Vector) at room temperature for 1 h and washed three times with phosphate-buffered saline. Alkaline phosphatase was used as the chromogen for 1 h. Next, the sections were counterstained with hematoxylin. Finally, dehydration and sealing of slices were performed as standard. No primary antibody was used in the negative control.

Trained pathologists count the number of positive cells in the appropriate fields per section to avoid the false positive inclusion of debris staining.

Data analysis

All spectrum data were used for principal component analysis (PCA) and linear discriminant analysis (LDA) in multivariate analysis, and data were presented as mean ± standard error of the mean (SEM). One-way ANOVA with *post hoc* Tukey's test was used throughout the study. $P < 0.05$ was considered statistically significant. ImageJ software was used for localization quantitation.

RESULTS

Coal dust exposure causes weight loss with lung inflammation and respiratory impairment

The body weight of mice in the CWP group decreased rapidly on the third day after exposure and was below baseline with continuous exposure on the 15th day before recovering slowly after the coal dust exposure stopped (Fig. 2A). Pulmonary function tests were carried out using whole-body plethysmography to evaluate the effect of coal dust exposure on mouse lung function. There was a significant difference in breathing frequency between the NS and CWP-3M groups (mean = 11,641, one-way ANOVA, $q = 4.018$, $p = 0.0368$, $n = 5$, df = 12). Consistently, the T_i/T_e ratios were significantly lower in the CWP-1M and CWP-3M groups than in the NS group (CWP-1M *vs* NS: mean = 0.5790, $q = 5.051$, $p = 0.0099$, $n = 5$, df = 12; CWP-3M *vs* NS: mean = 0.6087, $q = 4.398$, $p = 0.0228$, $n = 5$, df = 12). In the NS group, the mice had a balanced T_i/T_e ratio close to 1.0, with T_i and T_e of equal durations. However, after exposure to coal dust, the T_i/T_e ratio of the mice decreased, indicating an asymmetric breathing cycle. Overall, these results showed that mice in the CWP-1M and CWP-3M groups had declined lung functions. As shown in Fig. 2C, the inflammatory cells in the lung tissues of the mice in the NS group were slightly infiltrated, and the alveolar structure was normal. Inflammatory cell infiltration was found in the coal dust-exposed lung tissue of the CWP-1M group, and the alveolar structure was badly destroyed, with the tracheal wall thickening. Inflammatory cell infiltration was more apparent in the lungs of the CWP-3M group mice than in the CWP-1M group, especially around the trachea with the accumulation of coal dust particles and the interstitial inflammation was further aggravated (Fig. 2C).

Coal dust exposure causes changes in biochemical components detected by Raman spectroscopy

Confocal Raman microscopy was used to determine the effect of coal dust particles on lung tissues and detect the changes in these tissues' physical and chemical properties in the lung tissues of the three groups. In the CWP groups, the Raman spectra of lung tissue sections revealed a distinct band assignment indicating alterations in different cell components (Fig. 3A). The differences in Raman peak intensity across the groups reflected differences in cell metabolism and lung tissue components exposed to coal dust particles. Table 1 lists all of the band assignments detected by confocal Raman spectroscopy. Significant changes were evident in cholesterol (548 and 1,087 cm^{-1}), lipids (1,080 and 1,465 cm^{-1}), amino acids (750, 850, 1,004, 1,036, 1,123, and 1,552 cm^{-1}), nucleic acid (1,572 cm^{-1}), cytochrome C (746 cm^{-1}), and, most importantly, the fingerprint region (1,248 and 1,448 cm^{-1}), which represents collagen.

PCA (Fig. S1) and LDA (Fig. 3B) were used to reduce the dimension and highlight the spectral signatures of the different groups. The NS, CWP-1M, and CWP-3M groups were clearly separated by LD-1 and LD-2, which accounted for 17.4% of the variance
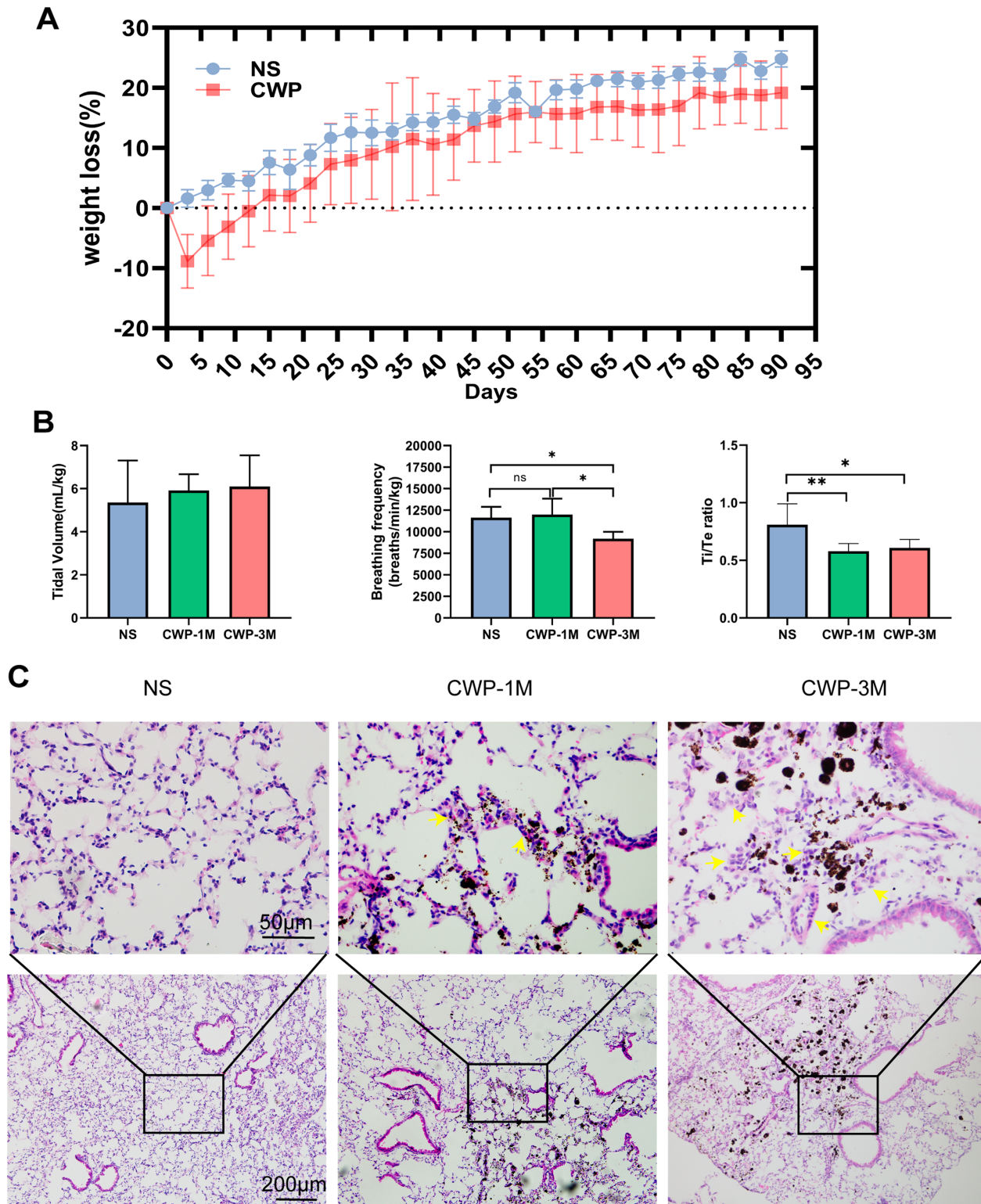
Figure 2 Exposure of mice to coal dust causes weight loss and induces apparent pulmonary inflammation. (A) Body weight was measured every 3 days. (B) Pulmonary tidal volume, breathing frequency, and the Ti/Te ratio after exposure of mice to coal dust particles. $n = 5$, $^*P < 0.05$, $^{**}P < 0.01$ *vs* the saline (NS) group. (C) Representative H & E staining of lung tissues from the different groups (400× magnification, scale bar = 50 μm; 200× magnification, scale bar = 200 μm). (NS, saline group; CWP-1M, coal dust exposure for 1 month; CWP-3M, coal dust exposure for 3 months).

Full-size 🖼 DOI: 10.7717/peerj.13632/fig-2
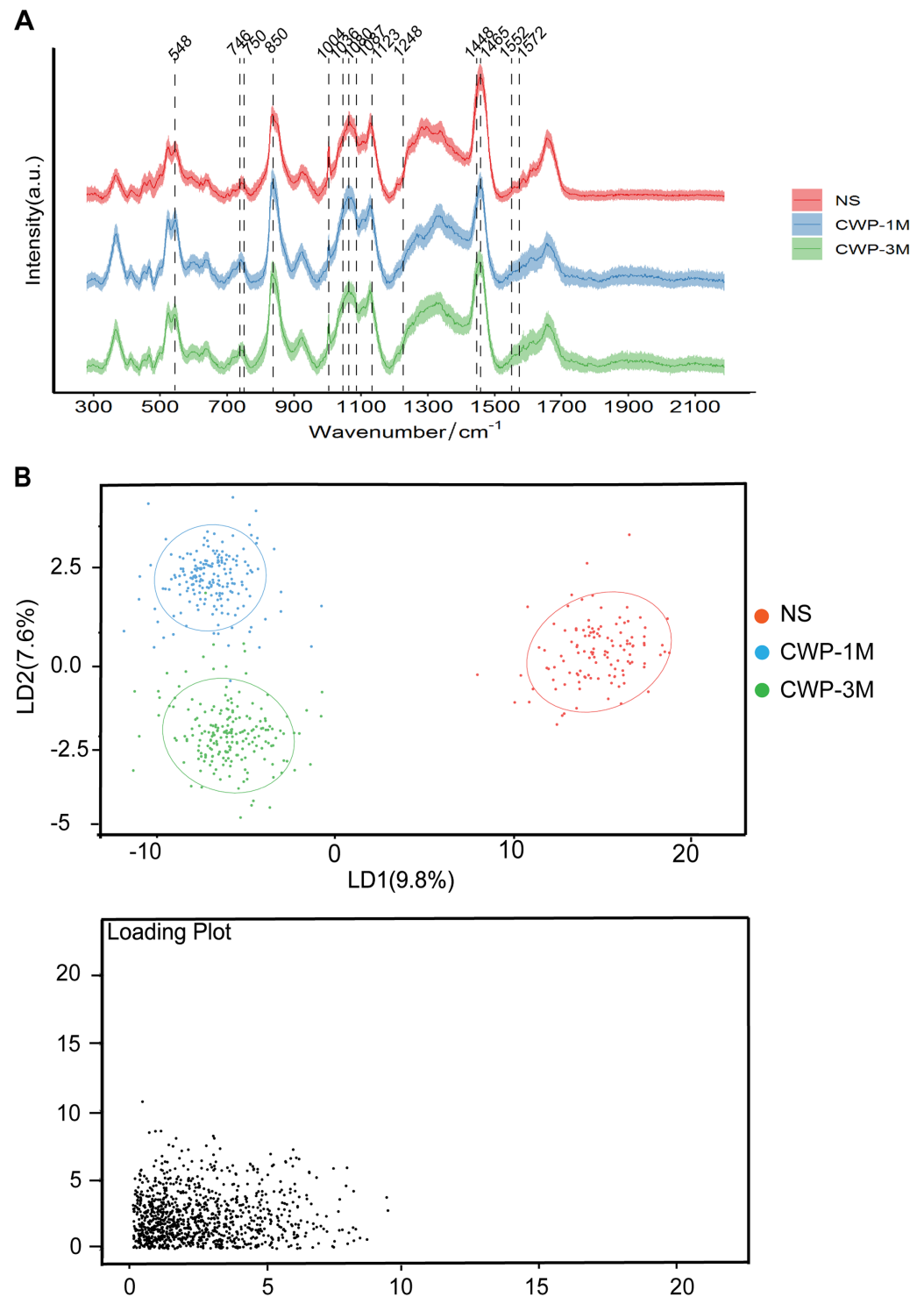
Figure 3 Coal dust exposure causes changes in the biochemical components detected by Raman spectroscopy. (A) The fingerprint regions of average Raman spectra collected from NS, CWP-1M, and CWP-3M mice. The variations in the Raman spectrum characteristics among the different groups are labeled. (B) LDA distinguished three groups. (NS, saline group; CWP-1M, coal dust exposure for 1 month; CWP-3M, coal dust exposure for 3 months). Full-size 🖼 DOI: 10.7717/peerj.13632/fig-3

Table 1 Assignment of specific Raman bands to vibrational modes and biological molecules.

Raman wavenumber (cm^{-1})	Biomolecule assignment	Molecular vibration	References
548	Cholesterol	Bending vibrations of (C–H)	*Czamara et al. (2015)*
746	Cytochrome C	ν(pyr breathing); ν(C-C)	*Okada et al. (2012), Zhang, Ge & Yu (2021)*
750	Tryptophan	Symmetric breathing	*Song et al. (2020a)*
850	Tyrosine, proline	ν(C-C), δ(CCH)ring breathing	*Song et al. (2020a)*
1,004	Phenylalanine	Ring breathing	*Sinica et al. (2019)*
1,036	Arginine	Cγ-Cδ bond	*Zhu et al. (2011)*
1,080	Typical phospholipids	P-O stretching vibration	*Malini et al. (2006)*
1,087	Cholesterol	C-C stretching	*Czamara et al. (2015)*
1,123	proteins	C-N stretching	*Song et al. (2020a)*
1,248	Collagen, proline	Amide III of β-sheet	*Song et al. (2020b)*
1,448	Collagen, phospholipids	δ(CH$_2$), δ(CH$_3$), δ(CH$_2$) scissoring	*Song et al. (2020a)*
1,465	Lipids	Amide I ν(C=C)	*Movasaghi, Rehman & Rehman (2007)*
1,552	Tryptophan	ν(C=C)	*Song et al. (2020a)*
1,572	Nucleic acids	Ring breathing modes in the DNA bases	*Song et al. (2020a)*

(Fig. 3B). LDA was able to discriminate cell populations better than PCA. The loading plots indicate those spectroscopic features most relevant for this variability.

Comparisons of the Raman band intensity among the different groups

To confirm the variations in lung tissue biomolecules among the different CWP and NS groups, we analyzed the significance of differences in band intensities (Fig. 4). The intensities of the 548 and 1,087 cm^{-1} cholesterol bands, a result of the bending vibrations of (C–H) and (C–C), were significantly higher in the CWP-1M group than in the NS group (548 cm^{-1}: mean = 0.1348, one-way ANOVA, q = 13.57, p < 0.0001, n = 188, df = 507; 1,087 cm^{-1}: mean = 0.1480, q = 5.761, p = 0.0002, n = 188, df = 507) and CWP-3M group (548 cm^{-1}: mean = 0.1348, one-way ANOVA, q = 11.93, p < 0.0001, n = 188, df = 507; 1,087 cm^{-1}: mean = 0.1480, one-way ANOVA, q = 5.402, p = 0.0004, n = 188, df = 507) (Fig. 4A). These bands reflect changes in cholesterol during cell metabolism and damage, which are reflected in the cell membrane indirectly (*Chakraborty et al., 2020*). This suggests that 1 month of coal dust exposure damaged the cell membranes. The same was seen for lipids but, interestingly, the intensity of the 1,465 cm^{-1} lipid band was significantly lower in the CWP-1M group than in the NS group (mean = 0.1981, one-way ANOVA, q = 28.67, p < 0.0001, n = 188, df = 507) and CWP-3M group (mean = 0.1981, one-way ANOVA, q = 11.53, p < 0.0001, n = 188, df = 507) (Fig. 4B). At the lipid band of 1,080 cm^{-1}, the intensity of that of the CWP-1M group was higher than that of the NS (mean = 0.1786, one-way ANOVA, q = 9.095, p < 0.0001, n = 188, df = 507) and CWP-3M group (mean = 0.1786, one-way ANOVA, q = 7.720, p = 0.0136, n = 188, df = 507), and there was no significant difference in the other two groups. This shows that the P–O stretching vibration can better represent the changes in the phospholipid bilayers of the lung tissue cell membrane.
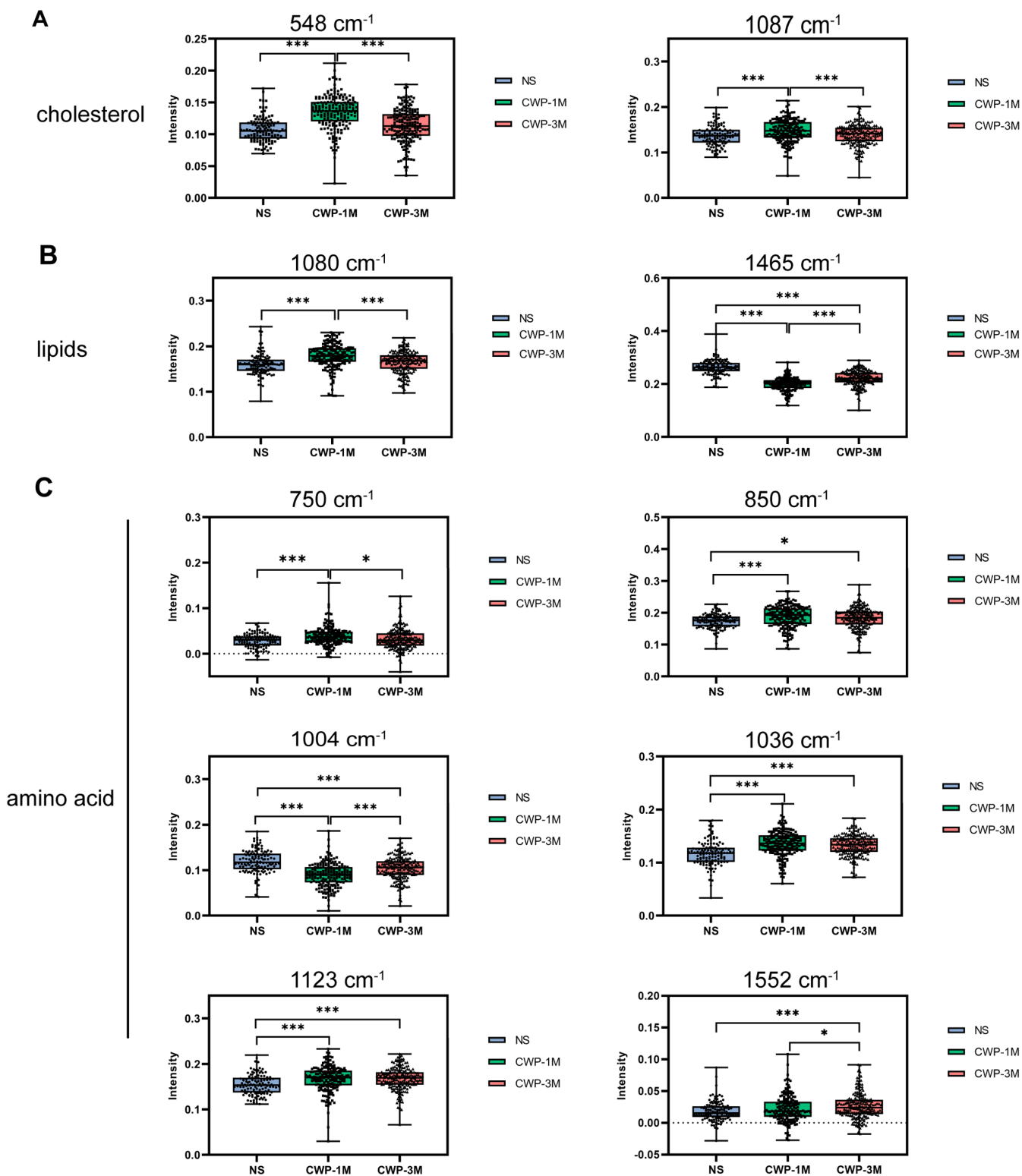
Figure 4 Comparisons of the Raman band intensity among different groups. Raman band intensities in the different groups were quantified to assess (A) cholesterol (548 and 1,087 cm^{-1}), (B) lipids (1,090 and 1,658 cm^{-1}), and (C) amino acids (750, 850, 1,004, 1,036, 1,123 and 1,552 cm^{-1}). One-way ANOVA with *post hoc* Tukey's test was used. The results represent means ± SEM. An asterisk (*) indicates $P < 0.05$, three asterisks (***) indicate $P \leq 0.001$. (NS, saline group; CWP-1M, coal dust exposure for 1 month; CWP-3M, coal dust exposure for 3 months).

Full-size 🖼 DOI: 10.7717/peerj.13632/fig-4
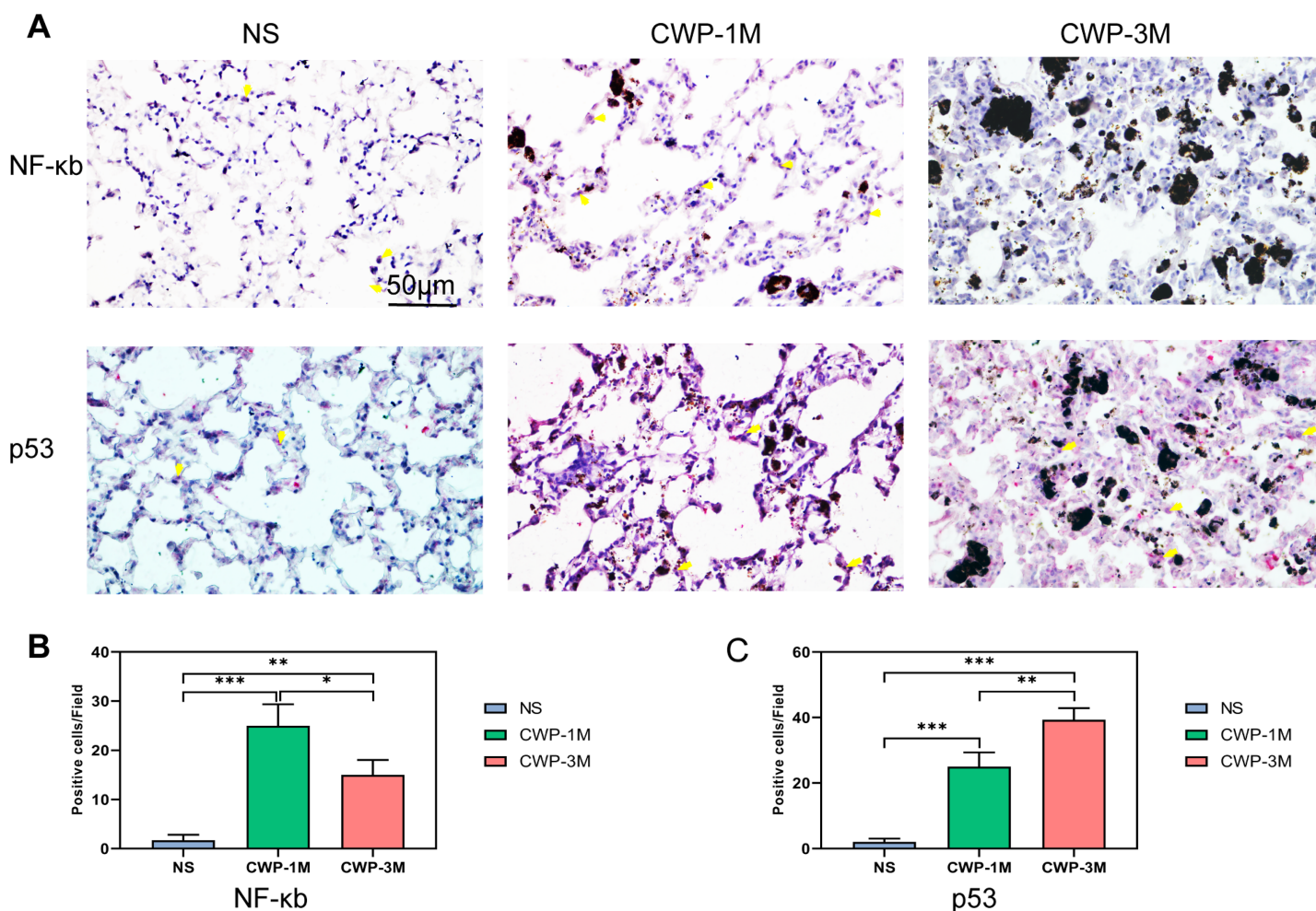
Figure 5 Coal dust exposure upregulates NF-κB and p53 expression in lung tissue. (A) NF-κB and p53 were detected in lung tissue from the different groups (400× magnification, scale bar = 50 μm). (B and C) Quantitative results of NF-κB-positive (B) and p53-positive (C) cells per three high-power fields. One-way ANOVA with *post hoc* Tukey's test was used. The results represent means ± SEM. An asterisk (*) indicates $P < 0.05$, two asterisks (**) indicate $P \leq 0.01$, three asterisks (***) indicate $P \leq 0.001$. (NS, saline group; CWP-1M, coal dust exposure for 1 month; CWP-3M, coal dust exposure for 3 months).

Full-size ⬛ DOI: 10.7717/peerj.13632/fig-5

The diverse types of amino acids in lung tissues were dramatically altered following coal dust exposure, as shown in Fig. 4C. The CWP-1M group had higher amino acid content than the NS group, as evidenced by variations in the intensity of the 750, 850, 1,036, 1,123, and 1,552 cm^{-1} bands. In contrast, in the CWP-1M group, phenylalanine, indicated by 1,004 cm^{-1}, was lower than in the other two groups.

Cholesterol and lipid as potential biomarkers of inflammation in CWP lungs

To further examine the results of the peak Raman spectra, we used immunohistochemical methods to more visually show the changes in the lung tissue after exposure to coal dust. As a key protein in the inflammatory response (*Lee et al., 2021a*), NF-κB was higher in the CWP-1M group than in the CWP-3M and NS groups and higher in the CWP-3M group than in the NS group (Figs. 5A and 5B). This suggests that there is more

inflammation during early exposure than later exposure. The results were consistent with the intensity of the 548 and 1,087 cm^{-1} cholesterol bands identified by confocal Raman spectroscopy (Fig. 4A). These results were also consistent with the 1,080 cm^{-1} lipid band. p53 is a particularly prominent transcriptional coregulator of TGF-β1 fibrosis response genes (*Higgins et al., 2021*). The expression of p53 was especially marked in the CWP-3M group (Figs. 5A and 5C), which was significantly higher than that in the CWP-1M and NS groups (CWP-3M *vs* CWP-1M, one-way ANOVA, $q = 7.562$, $p = 0.0042$, $n = 3$, df = 6; CWP-3M *vs* NS, one-way ANOVA, $q = 19.70$, $p < 0.0001$, $n = 3$, df = 6). These findings indicate cholesterol and lipid as potential biomarkers of lung inflammation in CWP lungs.

Potential biomarkers of lung proliferation and apoptosis in CWP lungs

To determine if coal dust can cause lung cell proliferation, we used Ki67 as an indicator of proliferation (*Jee et al., 2021*). The cell proliferation was significantly higher in the CWP-3M group than in the CWP-1M and NS groups. Similarly, the proliferation of the CWP-1M group was higher than that of the NS group (Figs. 6A and 6B). These results were consistent with the intensity of the 1,572 cm^{-1} nucleic acid band identified by confocal Raman spectroscopy (Fig. 6D). Interestingly, Bax, which is an apoptotic gene (*Zhaorigetu et al., 2021*), was significantly expressed in the CWP-1M group, but not in the CWP-3M group (Figs. 6A and 6C), and there was no significant difference between the NS and CWP-3M groups (mean = 2.00, one-way ANOVA, $q = 0.8464$, $p = 0.8261$, $n = 3$, df = 6). Similarly, this variation was consistent with the change in cytochrome C. Cytochrome C plays a very important role in cell apoptosis (*Zhang, Ge & Yu, 2021*), and the changes in cytochrome C showed increasing levels of apoptosis in CWP lungs (Fig. 6E). This phenomenon revealed that both cell proliferation and apoptosis are present in CWP groups, with apoptosis occurring in the early stage and proliferation present at all stages.

Pulmonary fibrosis and collagen accumulation caused by coal dust can be assessed by confocal Raman spectroscopy

We compared the results of traditional Masson's staining with Sirius Red staining to see if long-term exposure to coal dust particles can cause lung fibrosis (Fig. 7A). Meanwhile, we detected collagen characteristic spectra peaks in 1,248 and 1,448 cm^{-1}. As seen from the Masson's staining, more blue collagen fibers were identified in the lung of the CWP-3M group than in the CWP-1M group. In contrast, just a minor number of blue collagen fibers were found in the NS group. By using ImageJ software to calculate the percentage of blue collagen in the total lung tissue, it was found that the collagen content in the CWP-3M group was significantly higher than that in the CWP-1M and NS groups (CWP-3M *vs* CWP-1M: mean = 13.55, one-way ANOVA, $q = 13.13$, $p = 0.0002$, $n = 3$, df = 6, CWP-3M *vs* NS: mean = 13.55, one-way ANOVA, $q = 24.09$, $p < 0.0001$, $n = 3$, df = 6, Fig. 7B). With Sirius Red staining, type I collagen was yellow or red, type III collagen was green, and type II collagen was blue-green or grayish-blue under a polarizing microscope. As can be seen in Fig. 7A, the CWP-3M group had much more red and yellow
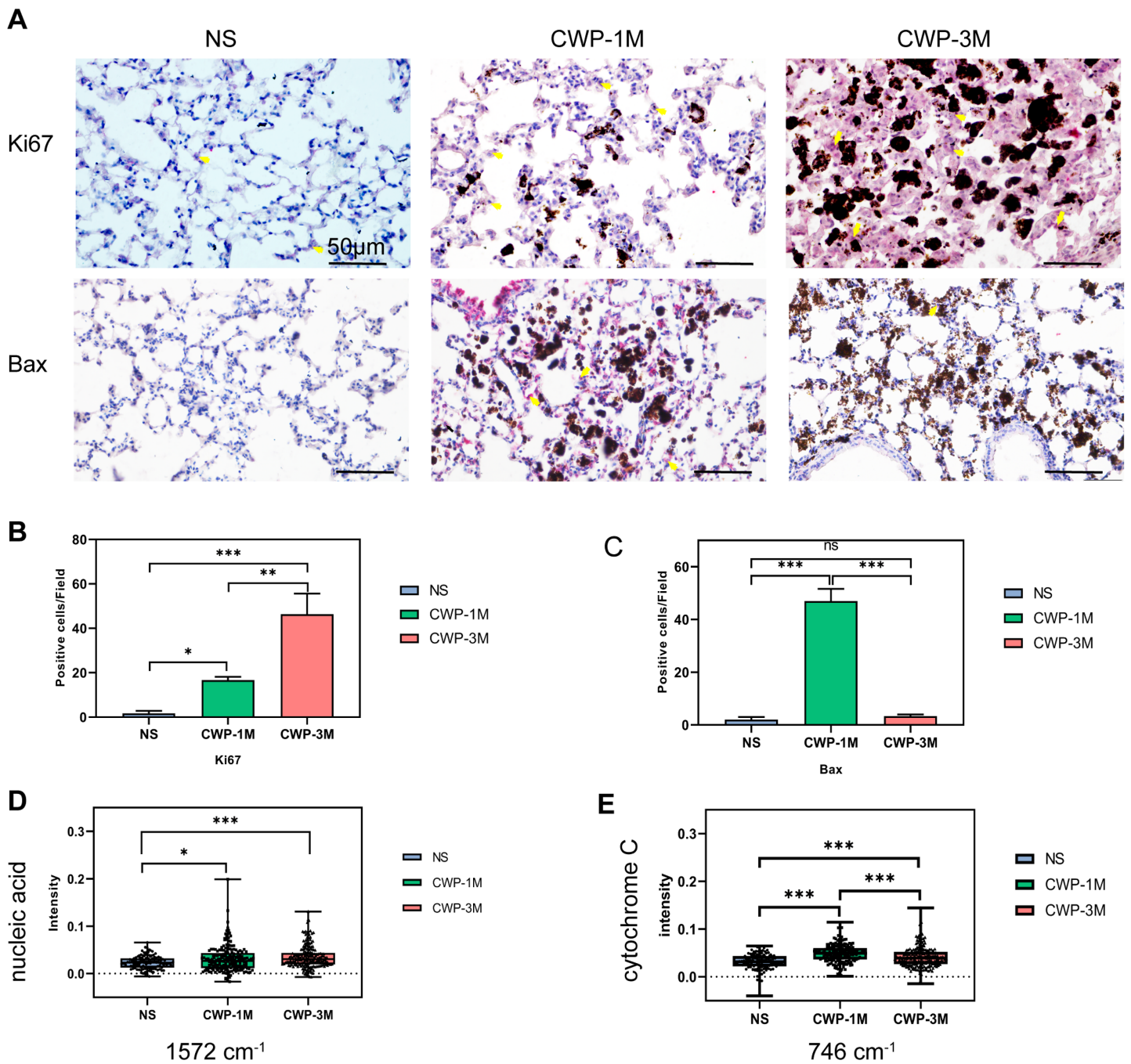
Figure 6 The Raman bands quantified to assess nucleic acid and cytochrome C were identified with Ki67 and Bax expression in lung tissue.
(A) Ki67 and Bax were detected in lung tissue from different groups (400× magnification, scale bar = 50 μm). (B and C) Quantitative results of Ki67-positive (B) and Bax-positive (C) cells per three high-power fields. (D and E) Intensity was semi-quantitatively analyzed to compare differences in the specific bands at (D) 1,572 cm^{-1} (nucleic acids) and (E) 746 cm^{-1} (cytochrome C) in different groups. One-way ANOVA with *post hoc* Tukey's test was used. The results represent means ± SEM. One asterisk (*) indicates $P < 0.05$, two asterisks (**) indicate $P \leq 0.01$, three asterisks (***) indicate $P \leq 0.001$. (NS, saline group; CWP-1M, coal dust exposure for 1 month; CWP-3M, coal dust exposure for 3 months).

Full-size 🖾 DOI: 10.7717/peerj.13632/fig-6

collagen than the CWP-1M and NS groups, and some of the collagen was coated with coal dust particles surrounding the trachea. The refraction of coal dust particles hampered the evaluation of tissue collagen by Sirius under polarized microscopy, which would affect the evaluation of collagen area by ImageJ (Fig. 7B).

Many studies have confirmed that Raman spectroscopy can evaluate collagen content according to the characteristic peak of collagen (*Bergholt, Serio & Albro, 2019*; *Janko et al., 2010*), and we selected the typical peaks of collagen in the lung tissues (1,248 and 1,448 cm^{-1}). The results showed that the collagen intensity of the 1,248 cm^{-1} band was significantly higher in the CWP-3M group than in the CWP-1M and NS groups. Similarly, the intensity of the 1,448 cm^{-1} collagen band was significantly higher in the CWP-3M group than in the CWP-1M and NS groups. The comparison of the peak strength of the collagen was consistent with that of Masson's staining.

DISCUSSION

Coal workers often inhale coal dust particles in the working environment, which can readily cause CWP. The pathological characteristics of CWP are pneumonia and pulmonary fibrosis (*Go & Cohen, 2020*), and our model showed that the lung tissue of mice was significantly damaged and altered by exposure to coal dust. For example, the collagen fibers of the tissue increased significantly over time, indicating that the lung tissue fibrosis caused by the coal dust progressed slowly, in contrast to that caused by silica, asbestos, and bleomycin (*Cao et al., 2021*; *Watanabe et al., 2021*). We take 16 mg coal dust to a mouse in a month, which is approximately a miner 10 to 20 years exposure (*Henneberger & Attfield, 1997*; *Borm & Tran, 2002*). These suggested that the mouse model was constructed in accordance with the development of CWP. Histopathological H&E staining showed that inflammatory cells infiltrated the lung tissue of mice exposed to coal dust and destroyed the alveolar structure. Over time, the inflammatory cell infiltration became more obvious, the bronchial wall thickened, the coal dust particles around the trachea accumulated more significantly, and the interstitial inflammation was further aggravated (Fig. 2C). These pathological changes in the lung tissue induced a pulmonary function decline in the mice. Overall, these results indicate that the early physical stimulation of lung tissue by coal dust particles causes a tissue-specific response, which is consistent with the model of early silica-induced pulmonary fibrosis (*Sai et al., 2021*; *Zhang et al., 2021*). As an important molecule in the inflammatory process (*Ng et al., 2021*; *Zhou et al., 2021*), the immunohistochemical expression of NF-κB in lung tissue was significantly increased, indicating that the inflammatory response of lung tissue was increased during coal dust exposure.

As a label-free detection technique, confocal Raman spectroscopy has considerable advantages in the molecular-level analysis of lung tissue. The differences in Raman intensities suggested alterations in cell metabolism and composition in lung tissue exposed to coal dust particles in the different groups. LDA demonstrated that confocal Raman spectroscopy could accurately differentiate normal and CWP lung tissue. Consistently, the changes in the biomolecules identified by Raman spectroscopy coincided with the immunohistochemical expression of various key molecules (Figs. 5 and 6). From the
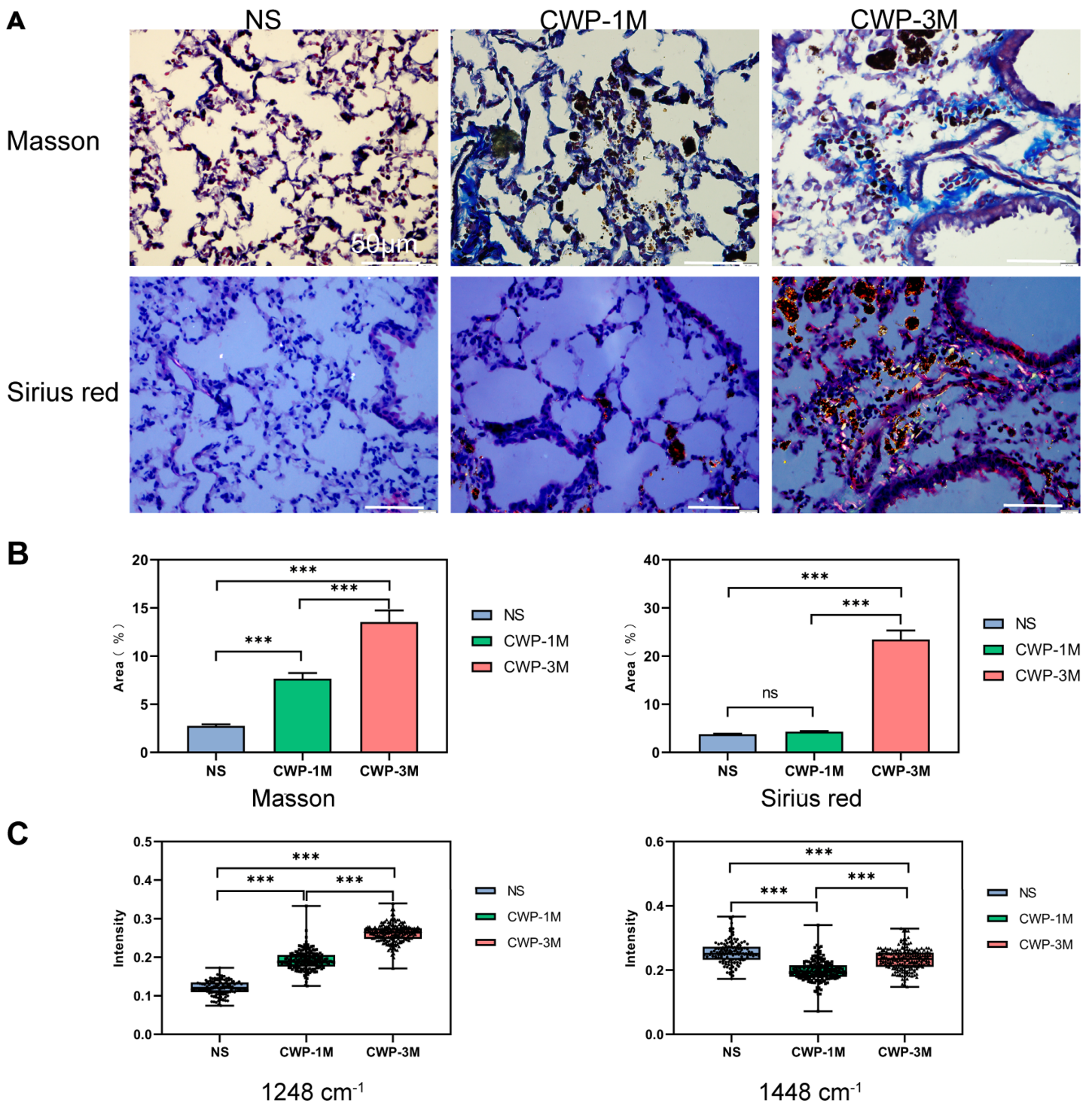
Figure 7 The Raman bands quantified to assess collagen changes were identified with Masson's staining and not Sirius Red staining.
(A) Representative images of Masson trichrome staining and Sirius Red staining for each group (400× magnification, scale bar = 50 µm).
(B) Quantification of the fibrotic area from Masson's staining and Sirius Red staining. (C) Raman band intensities in the different groups were
quantified to assess collagen (1,248 and 1,448 cm^{-1}). One-way ANOVA with *post hoc* Tukey's test was used. The results represent means ± SEM. ns
indicates $P \geq 0.05$, three asterisks (***) indicate $P \leq 0.001$.   Full-size DOI: 10.7717/peerj.13632/fig-7

inflammatory perspective, the expression of NF-κB was higher in CWP-1M lung tissues than in those of CWP-3M. This result suggests that the inflammation caused by coal dust exposure is gradually relieved, as also shown by the similar results for cholesterol. As a structural component that maintains membrane permeability and fluidity, cholesterol is essential for the function and integrity of mammalian cells. Inside the cell, cholesterol homeostasis is tightly controlled to ensure normal cellular processes (*Sèdes et al., 2018*). Besides, cholesterol homeostasis is highly regulated at the cellular level and interacts with G protein-coupled receptors (GPCRs), important receptors involved in protein-mediated signal transduction, affecting cell transport, metabolism, secretion, differentiation, growth, inflammation, and immune responses (*Pucadyil & Chattopadhyay, 2006*). Also, cholesterol ring peaks have been detected at 702 cm^{-1} (*Yue et al., 2014*), we did not observe the key peak, but using 548 and 1,087 cm^{-1}, cholesterol was also evaluated in the three groups. However, there are many prominent bands in the cholesterol spectrum (*Czamara et al., 2015*), particularly 548 and 1,087 cm^{-1}, associated with the C–C and C–H stretching modes (*Kočišová, Antalík & Procházka, 2013*; *Le Cacheux et al., 1996*) and which were consistent with NF-κB, and whether there is a corresponding trend in other inflammatory indicators needs further verification.

In addition, phospholipids and cholesterol play an important role in cell membrane stability and endoplasmic reticulum synthesis (*Krause & Regen, 2014*; *Lagace & Ridgway, 2013*). Compared among the three groups, it can be seen that the content of phospholipids at 1,080 cm^{-1} was the highest in the CWP-1M group, higher than in the NS group and CWP-3M group, and that the content of cholesterol was higher in the CWP-3M group than in the NS group. These findings indicate that, after coal dust exposure, considerable apoptosis occurred in the cells to resist the damage caused by the coal dust.

After 3 months of coal dust exposure, the tissue was in a repair state, and the cytochrome C results at 746 cm^{-1} were consistent with those of cholesterol. These results were also consistent with the immunohistochemical results of Bax. As one of the most important pro-apoptotic genes (*Zhaorigetu et al., 2021*), Bax expression was significantly upregulated in the CWP-1M group, while that in the NS and CWP-3M groups was almost at the baseline level, showing that the CWP-1M group had the highest level of apoptosis. The changes in cytochrome C (746 cm^{-1}), which can also represent apoptosis, were also correlated with the changes in cholesterol and phospholipids. The upregulation of Bax can lead to the release of cytochrome C, thereby inducing apoptosis. The release of cytochrome C from mitochondria is the key event of apoptosis (*Gama et al., 2014*). Interestingly, the Amide I ν(C=C) lipid band represented by 1,465 cm^{-1} was not consistent with the change in the phospholipid peak of 1,080 cm^{-1}, indicating that P–O stretching vibration could better represent the change in the phospholipid of the lung tissue cell membrane in this study.

Amino acid synthesis and catabolic metabolism are interweaved with cell redox homeostasis (*Vettore, Westbrook & Tennant, 2020*), with the changes in the different amino acids (bands at 750, 850, 1,004, 1,036, 1,123, and 1,552 cm^{-1}) shown on Raman

spectra indicating active cellular metabolism in lung tissue. We observed an increase in amino acid signal, but a reduction in the phenylalanine peak at 1,004 cm^{-1}. The contradictory phenomenon may indicate that coal dust causes amino acid metabolism disorder in lung tissue (*Chen et al., 2020*; *Engelen & Schols, 2003*). As a related antigen of proliferating cells, Ki67 is closely linked to mitosis and is indispensable in cell proliferation (*Plantier et al., 2018*). Our immunohistochemical results for Ki67 showed that active lung tissue proliferation was higher in the CWP-3M group than in the CWP-1M and NS groups. *El-Zammar, Rosenbaum & Katzenstein (2009)* suggested that the low proliferative activity of fibroblasts in common interstitial pneumonia and scar tissue supported the hypothesis of abnormal wound healing in common interstitial pneumonia. Therefore, future studies will focus on the cell types undergoing proliferation in the CWP-1M and CWP-3M groups. The nucleic acid peak at 1,572 cm^{-1} also indicated that the cells exhibited clear proliferation after coal dust exposure. The intensity of the 783–790 cm^{-1} Raman spectra were very weak with no apparent Raman signal. These peaks do not corroborate the analysis at 1,572 cm^{-1}. A total of 1,572 cm^{-1} represent "Ring breathing modes in the DNA bases", and 786 cm^{-1} represent "symmetric phosphodiester stretch or ring breathing modes of pyrimidine bases", the reason for this difference may be due to the influence of molecular structure. We concluded that 1,572 cm^{-1} was more representative for the nucleic acid peak in lung tissues (*Song et al., 2020a*). The Raman spectra of nucleic acid may have different exhibitions at the cell proliferation early-stage and late-stage when cells proliferate, 1,572 cm^{-1} indicating the cell in the early stage of proliferation (*Su et al., 2017*).

Coal dust exposure caused an increase in collagen, which is an important component of the extracellular matrix. In our study, Masson's staining can evaluate collagen very well but, due to the auto-fluorescence of coal dust particles (*Yang et al., 2020*), Sirius Red staining can lead to biased results under polarizing microscopy, which is why we believe that Sirius Red staining cannot adequately evaluate collagen content. Collagen peak intensities of 1,248 and 1,448 cm^{-1} can be used to determine the collagen content of tissues. Although, most lipid species produce characteristic CH2 modes at 1,440–1,448 cm^{-1} (*Movasaghi, Rehman & Rehman, 2007*), we assign the 1,448 cm^{-1} to collagen (*Song et al., 2020a*), which is consistent with the Masson's staining results. Thus, confocal Raman spectroscopy has advantages in evaluating the fibrosis degree of lung tissues exposed to coal dust.

CONCLUSIONS

In summary, confocal Raman spectroscopy revealed major changes in biochemical molecules associated with coal pneumoconiosis. To our knowledge, we are the first to use confocal Raman spectroscopy to analyze the biochemical changes in the CWP lungs. This approach will help expand our understanding of the toxicity of coal dust in the lung. In addition, we described cholesterol, lipid, nucleic acid, cytochrome C, and collagen band detected by Raman spectroscopy as potential biomarkers of inflammatory, proliferation, cell apoptosis, and collagen fibers in CWP lungs.

ADDITIONAL INFORMATION AND DECLARATIONS

Competing Interests

The authors declare that they have no competing interests.

Author Contributions

- Wenyang Wang performed the experiments, analyzed the data, prepared figures and/or tables, authored or reviewed drafts of the article, and approved the final draft.
- Min Mu conceived and designed the experiments, authored or reviewed drafts of the article, and approved the final draft.
- Yuanjie Zou performed the experiments, analyzed the data, prepared figures and/or tables, and approved the final draft.
- Bing Li analyzed the data, authored or reviewed drafts of the article, and approved the final draft.
- Hangbing Cao performed the experiments, prepared figures and/or tables, authored or reviewed drafts of the article, and approved the final draft.
- Dong Hu conceived and designed the experiments, authored or reviewed drafts of the article, and approved the final draft.
- Xinrong Tao conceived and designed the experiments, authored or reviewed drafts of the article, and approved the final draft.

Animal Ethics

The following information was supplied relating to ethical approvals (*i.e.*, approving body and any reference numbers):

Anhui University of Science and Technology.

Data Availability

The following information was supplied regarding data availability:

The raw measurements are all available in the Supplemental Files.

Supplemental Information

Supplemental information for this article can be found online at http://dx.doi.org/10.7717/peerj.13632#supplemental-information.

REFERENCES

Albrecht C, Borm PJA, Adolf B, Timblin CR, Mossman BT. 2002. In vitro and in vivo activation of extracellular signal-regulated kinases by coal dusts and quartz silica. *Toxicology and Applied Pharmacology* **184(1)**:37–45 DOI 10.1006/taap.2002.9500.

Bergholt MS, Serio A, Albro MB. 2019. Raman spectroscopy: guiding light for the extracellular matrix. *Frontiers in Bioengineering and Biotechnology* **7**:303 DOI 10.3389/fbioe.2019.00303.

Borm PJA, Tran L. 2002. From quartz hazard to quartz risk: the coal mines revisited. *The Annals of Occupational Hygiene* **46**:25–32 DOI 10.1093/annhyg/mef021.

Cao Z-J, Liu Y, Zhang Z, Yang P-R, Li Z-G, Song M-Y, Qi X-M, Han Z-F, Pang J-L, Li B-C, Zhang X-R, Dai H-P, Wang J, Wang C. 2021. Pirfenidone ameliorates silica-induced lung inflammation and fibrosis in mice by inhibiting the secretion of interleukin-17A. *Acta Pharmacologica Sinica* **43(4)**:908–918 DOI 10.1038/s41401-021-00706-4.

Chakraborty S, Doktorova M, Molugu TR, Heberle FA, Scott HL, Dzikovski B, Nagao M, Stingaciu L-R, Standaert RF, Barrera FN, Katsaras J, Khelashvili G, Brown MF, Ashkar R. 2020. How cholesterol stiffens unsaturated lipid membranes. *Proceedings of the National Academy of Sciences of the United States of America* **117(36)**:21896–21905 DOI 10.1073/pnas.2004807117.

Chen J, Jin Y, Yang Y, Wu Z, Wu G. 2020. Epithelial dysfunction in lung diseases: effects of amino acids and potential mechanisms. *Advances in Experimental Medicine and Biology* **1265**:57–70 DOI 10.1007/978-3-030-45328-2.

Czamara K, Majzner K, Pacia MZ, Kochan K, Kaczor A, Baranska M. 2015. Raman spectroscopy of lipids: a review. *Journal of Raman Spectroscopy* **46(1)**:4–20 DOI 10.1002/jrs.4607.

El-Zammar O, Rosenbaum P, Katzenstein A-LA. 2009. Proliferative activity in fibrosing lung diseases: a comparative study of Ki-67 immunoreactivity in diffuse alveolar damage, bronchiolitis obliterans–organizing pneumonia, and usual interstitial pneumonia. *Human Pathology* **40(8)**:1182–1188 DOI 10.1016/j.humpath.2009.01.006.

Engelen MPKJ, Schols AMWJ. 2003. Altered amino acid metabolism in chronic obstructive pulmonary disease: new therapeutic perspective? *Current Opinion in Clinical Nutrition and Metabolic Care* **6(1)**:73–78 DOI 10.1097/00075197-200301000-00011.

Finnerty K, Choi J-E, Lau A, Davis-Gorman G, Diven C, Seaver N, Linak WP, Witten M, McDonagh PF. 2007. Instillation of coarse ash particulate matter and lipopolysaccharide produces a systemic inflammatory response in mice. *Journal of Toxicology and Environmental Health, Part A* **70(23)**:1957–1966 DOI 10.1080/15287390701549229.

Gama V, Swahari V, Schafer J, Kole AJ, Evans A, Huang Y, Cliffe A, Golitz B, Sciaky N, Pei X-H, Xiong Y, Deshmukh M. 2014. The E3 ligase PARC mediates the degradation of cytosolic cytochrome c to promote survival in neurons and cancer cells. *Science Signaling* **7(334)**:ra67 DOI 10.1126/scisignal.2005309.

Go L, Cohen RA. 2020. Coal workers' pneumoconiosis and other mining-related lung disease. *Clinics in Chest Medicine* **41(4)**:687–696 DOI 10.1016/j.ccm.2020.08.002.

Happo MS, Hirvonen M-R, Halinen AI, Jalava PI, Pennanen AS, Sillanpaa M, Hillamo R, Salonen RO. 2008. Chemical compositions responsible for inflammation and tissue damage in the mouse lung by coarse and fine particulate samples from contrasting air pollution in Europe. *Inhalation Toxicology* **20(14)**:1215–1231 DOI 10.1080/08958370802147282.

Hargrove MM, McGee JK, Gibbs-Flournoy EA, Wood CE, Kim YH, Gilmour MI, Gavett SH. 2018. Source-apportioned coarse particulate matter exacerbates allergic airway responses in mice. *Inhalation Toxicology* **30(11–12)**:405–415 DOI 10.1080/08958378.2018.1542047.

Henneberger PK, Attfield MD. 1997. Respiratory symptoms and spirometry in experienced coal miners: effects of both distant and recent coal mine dust exposures. *American Journal of Industrial Medicine* **32**:268–274 DOI 10.1002/(ISSN)1097-0274.

Higgins CE, Tang J, Higgins SP, Gifford CC, Mian BM, Jones DM, Zhang W, Costello A, Conti DJ, Samarakoon R, Higgins PJ. 2021. The genomic response to TGF-β1 dictates failed repair and progression of fibrotic disease in the obstructed kidney. *Frontiers in Cell and Developmental Biology* **9**:678524 DOI 10.3389/fcell.2021.678524.

Hsu C-C, Xu J, Brinkhof B, Wang H, Cui Z, Huang WE, Ye H. 2020. A single-cell Raman-based platform to identify developmental stages of human pluripotent stem cell-derived neurons. *Proceedings of the National Academy of Sciences of the United States of America* **117(31)**:18412–18423 DOI 10.1073/pnas.2001906117.

Janko M, Davydovskaya P, Bauer M, Zink A, Stark RW. 2010. Anisotropic Raman scattering in collagen bundles. *Optics Letters* **35(16)**:2765–2767 DOI 10.1364/OL.35.002765.

Jee S, Kim H, Bang S, Kim Y, Park HY, Paik SS, Sim J, Jang K. 2021. Low-level expression of MTUS1 is associated with poor survival in patients with lung adenocarcinoma. *Diagnostics* **11(7)**:1250 DOI 10.3390/diagnostics11071250.

Kang JW, Nguyen FT, Lue N. 2021. Temporal imaging of live cells by high-speed confocal Raman microscopy. *Materials* **14(13)**:3732 DOI 10.3390/ma14133732.

Kočišová E, Antalík A, Procházka M. 2013. Drop coating deposition Raman spectroscopy of liposomes: role of cholesterol. *Chemistry and Physics of Lipids* **172–173**:1–5 DOI 10.1016/j.chemphyslip.2013.04.002.

Krause MR, Regen SL. 2014. The structural role of cholesterol in cell membranes: from condensed bilayers to lipid rafts. *Accounts of Chemical Research* **47(12)**:3512–3521 DOI 10.1021/ar500260t.

Lagace TA, Ridgway ND. 2013. The role of phospholipids in the biological activity and structure of the endoplasmic reticulum. *Biochimica et Biophysica Acta (BBA) - Molecular Cell Research* **1833(11)**:2499–2510 DOI 10.1016/j.bbamcr.2013.05.018.

Le Cacheux P, Ménard G, Nguyen Quang H, Dao NQ, Roach AG, Dron D. 1996. Quantitative determination of free and esterified cholesterol concentrations in cholesterol-fed rabbit aorta using near-infrared- Fourier transform-Raman spectroscopy. *Spectrochimica Acta Part A: Molecular and Biomolecular Spectroscopy* **52(12)**:1619–1627 DOI 10.1016/0584-8539(96)01738-2.

Lee SM, Son K-N, Shah D, Ali M, Balasubramaniam A, Shukla D, Aakalu VK. 2021a. Histatin-1 attenuates LPS-induced inflammatory signaling in RAW264.7 macrophages. *International Journal of Molecular Sciences* **22(15)**:7856 DOI 10.3390/ijms22157856.

Lee YY, Yang W-K, Han JE, Kwak D, Kim T-H, Saba E, Kim S-D, Lee Y-C, Kim JS, Kim S-H, Rhee MH. 2021b. Hypericum ascyron L. extract reduces particulate matter-induced airway inflammation in mice. *Phytotherapy Research* **35(3)**:1621–1633 DOI 10.1002/ptr.6929.

León-Mejía G, Machado MN, Okuro RT, Silva LFO, Telles C, Dias J, Niekraszewicz L, Da Silva J, Henriques JAP, Zin WA. 2018. Intratracheal instillation of coal and coal fly ash particles in mice induces DNA damage and translocation of metals to extrapulmonary tissues. *The Science of the Total Environment* **625(1)**:589–599 DOI 10.1016/j.scitotenv.2017.12.283.

Li Y, Shen R, Wu H, Yu L, Wang Z, Wang D. 2020. Liver changes induced by cadmium poisoning distinguished by confocal Raman imaging. *Spectrochimica Acta Part A: Molecular and Biomolecular Spectroscopy* **225(10)**:117483 DOI 10.1016/j.saa.2019.117483.

Lu J, Chen J, Liu C, Zeng Y, Sun Q, Li J, Shen Z, Chen S, Zhang R. 2022. Identification of antibiotic resistance and virulence-encoding factors in Klebsiella pneumoniae by Raman spectroscopy and deep learning. *Microbial Biotechnology* **15(4)**:1270–1280 DOI 10.1111/1751-7915.13960.

Malini R, Venkatakrishna K, Kurien J, Pai KM, Rao L, Kartha VB, Krishna CM. 2006. Discrimination of normal, inflammatory, premalignant, and malignant oral tissue: a Raman spectroscopy study. *Biopolymers* **81**:179–193 DOI 10.1002/bip.20398.

Movasaghi Z, Rehman S, Rehman I. 2007. Raman spectroscopy of biological tissues. *Applied Spectroscopy Reviews* **42(5)**:493–541 DOI 10.1080/05704920701551530.

Mu M, Li B, Zou Y, Wang W, Cao H, Zhang Y, Sun Q, Chen H, Ge D, Tao H, Hu D, Yuan L, Tao X, Wang J. 2022. Coal dust exposure triggers heterogeneity of transcriptional profiles in mouse pneumoconiosis and Vitamin D remedies. *Particle and Fibre Toxicology* **19(1)**:7 DOI 10.1186/s12989-022-00449-y.

Ng B, Widjaja AA, Viswanathan S, Dong J, Chothani SP, Lim S, Shekeran SG, Tan J, McGregor NE, Walker EC, Sims NA, Schafer S, Cook SA. 2021. Similarities and differences between IL11 and IL11RA1 knockout mice for lung fibro-inflammation, fertility and craniosynostosis. *Scientific Reports* **11(1)**:14088 DOI 10.1038/s41598-021-93623-9.

Okada M, Smith NI, Palonpon AF, Endo H, Kawata S, Sodeoka M, Fujita K. 2012. Label-free Raman observation of cytochrome c dynamics during apoptosis. *Proceedings of the National Academy of Sciences of the United States of America* **109**:28 DOI 10.1073/pnas.1107524108.

Perret JL, Plush B, Lachapelle P, Hinks TSC, Walter C, Clarke P, Irving L, Brady P, Dharmage SC, Stewart A. 2017. Coal mine dust lung disease in the modern era. *Respirology* **22(4)**:662–670 DOI 10.1111/resp.13034.

Plantier L, Cazes A, Dinh-Xuan A-T, Bancal C, Marchand-Adam S, Crestani B. 2018. Physiology of the lung in idiopathic pulmonary fibrosis. *European Respiratory Review* **27(147)**:170062 DOI 10.1183/16000617.0062-2017.

Pucadyil TJ, Chattopadhyay A. 2006. Role of cholesterol in the function and organization of G-protein coupled receptors. *Progress in Lipid Research* **45(4)**:295–333 DOI 10.1016/j.plipres.2006.02.002.

Sai L, Qi X, Yu G, Zhang J, Zheng Y, Jia Q, Peng C. 2021. Dynamic assessing silica particle-induced pulmonary fibrosis and associated regulation of long non-coding RNA expression in Wistar rats. *Genes and Environment* **43(1)**:23 DOI 10.1186/s41021-021-00193-3.

Sinica A, Brožáková K, Brůha T, Votruba J. 2019. Raman spectroscopic discrimination of normal and cancerous lung tissues. *Spectrochimica Acta Part A: Molecular and Biomolecular Spectroscopy* **219**:257–266 DOI 10.1016/j.saa.2019.04.055.

Song D, Chen T, Wang S, Chen S, Li H, Yu F, Zhang J, Zhang Z. 2020a. Study on the biochemical mechanisms of the micro-wave ablation treatment of lung cancer by ex vivo confocal Raman microspectral imaging. *The Analyst* **145(2)**:626–635 DOI 10.1039/C9AN01524H.

Song D, Yu F, Chen S, Chen Y, He Q, Zhang Z, Zhang J, Wang S. 2020b. Raman spectroscopy combined with multivariate analysis to study the biochemical mechanism of lung cancer microwave ablation. *Biomedical Optics Express* **11**:1061–1072 DOI 10.1364/BOE.383869.

Su X, Fang S, Zhang D, Zhang Q, Lu X, Tian J, Fan J, Zhong L. 2017. Raman spectrum reveals Mesenchymal stem cells inhibiting HL60 cells growth. *Spectrochimica Acta Part A: Molecular and Biomolecular Spectroscopy* **177**(Suppl. 5):15–19 DOI 10.1016/j.saa.2017.01.021.

Sun L, Fan M, Huang D, Li B, Xu R, Gao F, Chen Y. 2021. Clodronate-loaded liposomal and fibroblast-derived exosomal hybrid system for enhanced drug delivery to pulmonary fibrosis. *Biomaterials* **271**(10082):120761 DOI 10.1016/j.biomaterials.2021.120761.

Sèdes L, Thirouard L, Maqdasy S, Garcia M, Caira F, Lobaccaro J-MA, Beaudoin C, Volle DH. 2018. Cholesterol: a gatekeeper of male fertility? *Frontiers in Endocrinology* **9**:369 DOI 10.3389/fendo.2018.00369.

Vettore L, Westbrook RL, Tennant DA. 2020. New aspects of amino acid metabolism in cancer. *British Journal of Cancer* **122**(2):150–156 DOI 10.1038/s41416-019-0620-5.

Wang W, Mu M, Zou Y, Li B, Cao H, Hu D, Tao X. 2022. Label-free Raman spectroscopy characterizes signatures of inflammation and fibrosis in the silicosis. *Biochemical and Biophysical Research Communications* **606**:114–120 DOI 10.1016/j.bbrc.2022.03.107.

Watanabe S, Markov NS, Lu Z, Piseaux Aillon R, Soberanes S, Runyan CE, Ren Z, Grant RA, Maciel M, Abdala-Valencia H, Politanska Y, Nam K, Sichizya L, Kihshen HG, Joshi N, McQuattie-Pimentel AC, Gruner KA, Jain M, Sznajder JI, Morimoto RI, Reyfman PA, Gottardi CJ, Budinger GRS, Misharin AV. 2021. Resetting proteostasis with ISRIB promotes epithelial differentiation to attenuate pulmonary fibrosis. *Proceedings of the National Academy of Sciences of the United States of America* **118**(20):e2101100118 DOI 10.1073/pnas.2101100118.

Wen J, Tang T, Kanwal S, Lu Y, Tao C, Zheng L, Zhang D, Gu Z. 2021. Detection and classification of multi-type cells by using confocal raman spectroscopy. *Frontiers in Chemistry* **9**:641670 DOI 10.3389/fchem.2021.641670.

Yang Y, Qin J, Qi T, Zhou X, Chen R, Tan J, Xiao K, Ji D, He K, Chen X. 2020. Fluorescence characteristics of particulate water-soluble organic compounds emitted from coal-fired boilers. *Atmospheric Environment* **223**(2):117297 DOI 10.1016/j.atmosenv.2020.117297.

Yuan J, Wang T, Wang L, Li P, Shen H, Mo Y, Zhang Q, Ni C. 2022. Transcriptome-wide association study identifies PSMB9 as a susceptibility gene for coal workers' pneumoconiosis. *Environmental Toxicology* **11**(5):474 DOI 10.1002/tox.23554.

Yue S, Li J, Lee S-Y, Lee HJ, Shao T, Song B, Cheng L, Masterson TA, Liu X, Ratliff TL, Cheng J-X. 2014. Cholesteryl ester accumulation induced by PTEN loss and PI3K/AKT activation underlies human prostate cancer aggressiveness. *Cell Metabolism* **19**(3):393–406 DOI 10.1016/j.cmet.2014.01.019.

Zhang J, Ge W, Yu Q. 2021. Structural evaluation of cytochrome c by Raman spectroscopy and its relationship with apoptosis and protein degradation in postmortem bovine muscle. *Food Chemistry* **362**(1):130189 DOI 10.1016/j.foodchem.2021.130189.

Zhang E, Geng X, Shan S, Li P, Li S, Li W, Yu M, Peng C, Wang S, Shao H, Du Z. 2021. Exosomes derived from bone marrow mesenchymal stem cells reverse epithelial-mesenchymal transition potentially via attenuating Wnt/β-catenin signaling to alleviate silica-induced pulmonary fibrosis. *Toxicology Mechanisms and Methods* **31**(9):655–666 DOI 10.1080/15376516.2021.1950250.

Zhaorigetu, Farrag IM, Belal A, Badawi MHA, Abdelhady AA, Galala FMAA, El-Sharkawy A, El-Dahshan AA, Mehany ABM. 2021. Antiproliferative, apoptotic effects and suppression of

oxidative stress of quercetin against induced toxicity in lung cancer cells of rats: in vitro and in vivo study. *Journal of Cancer* **12(17)**:5249–5259 DOI 10.7150/jca.52088.

Zhou Z, Choi J-W, Shin JY, Kim D-U, Kweon B, Oh H, Kim Y-C, Song H-J, Bae G-S, Park S-J. 2021. Betulinic acid ameliorates the severity of acute pancreatitis via inhibition of the NF-κB signaling pathway in mice. *International Journal of Molecular Sciences* **22(13)**:6871 DOI 10.3390/ijms22136871.

Zhu G, Zhu X, Fan Q, Wan X. 2011. Raman spectra of amino acids and their aqueous solutions. *Spectrochimica Acta Part A: Molecular and Biomolecular Spectroscopy* **78**:1187–1195 DOI 10.1016/j.saa.2010.12.079.

Zitouni N, Bousserrhine N, Belbekhouche S, Missawi O, Alphonse V, Boughatass I, Banni M. 2020. First report on the presence of small microplastics (≤3 μm) in tissue of the commercial fish Serranus scriba (Linnaeus. 1758) from Tunisian coasts and associated cellular alterations. *Environmental Pollution* **263(4)**:114576 DOI 10.1016/j.envpol.2020.114576.